HUMAN-ROBOT INTERACTION

Surface haptic rendering of virtual shapes through change in surface temperature

Changhyun Choi[1]†, Yuan Ma[1,2,3]*†, Xinyi Li[1], Sitangshu Chatterjee[1], Sneha Sequeira[1], Rebecca F. Friesen[1], Jonathan R. Felts[1], M. Cynthia Hipwell[1]*

Compared to relatively mature audio and video human-machine interfaces, providing accurate and immersive touch sensation remains a challenge owing to the substantial mechanical and neurophysical complexity of touch. Touch sensations during relative lateral motion between a skin-screen interface are largely dictated by interfacial friction, so controlling interfacial friction has the potential for realistic mimicry of surface texture, shape, and material composition. In this work, we show a large modulation of finger friction by locally changing surface temperature. Experiments showed that finger friction can be increased by ~50% with a surface temperature increase from 23° to 42°C, which was attributed to the temperature dependence of the viscoelasticity and the moisture level of human skin. Rendering virtual features, including zoning and bump(s), without thermal perception was further demonstrated with surface temperature modulation. This method of modulating finger friction has potential applications in gaming, virtual and augmented reality, and touchscreen human-machine interaction.

INTRODUCTION

The haptics market is rapidly growing thanks to the expanding need for immersive human-machine interfaces. Applications—including teleoperation, remote collaboration, virtual reality (VR), and augmented reality—benefit from incorporating the sense of touch through cutaneous and kinesthetic channels in delivering more realistic feedback for human-machine interactions (*1*–*8*). Mechanical and electrical stimuli are most commonly used for haptic feedback. Most mechanical stimuli deform the skin tissue by normal or lateral force modulations (*9*), whereas electrotactile stimuli activate the nerve fibers of mechanoreceptors through the application of a small current (*10*).

Surface haptic devices (SHDs) have an interactive touch surface that provides the users with tactile feedback on a surface (*9*) and enable functions that are not possible with traditional touchscreens, such as texture rendering, virtual knobs, and virtual buttons (*11*–*13*). Current SHDs work by vibrating the surface at an ultrasonic frequency or attracting the skin using an electrostatic effect called electroadhesion (*14*, *15*). Ultrasonic vibration decreases friction force by creating a lubricating squeeze film using surface vibration, whereas electroadhesion increases friction forces using high-voltage electrostatic interaction (typically 100 to 500 V) between fingertips and screens (*16*, *17*). The current commercially available devices can achieve 15 to 30% increase over the base friction force with typical voltages of 100 to 200 V (*18*–*25*). Higher friction modulation of up to 43% has also been demonstrated with higher driving voltages of 200 to 500 V (*26*–*28*).

Both of these approaches, however, face different challenges in their applications. Ultrasonic devices consume a large amount of power when vibrating entire screen surfaces to generate sufficient friction reduction and also require special structural designs that confine and withstand the ultrasonic vibration. The uniformity of vibration is also challenged by the intrinsic vibration modes of the structure (*9*). Electroadhesion-based SHDs, on the other hand, require high-voltage circuitry to generate sufficient force between the fingertip and screen, which increases the cost of the device (*9*). Thus, alternative methods of lateral force modulation that are low voltage and efficiently localize the haptic effect on a surface are highly desirable.

In this work, we propose a method to modulate finger friction using changes in surface temperature to induce changes in the mechanical response of the sliding finger in contact (Fig. 1). This work was inspired by previous research studying the temperature-dependent friction behavior of polymeric solids like rubbers (*29*, *30*). Here, we hypothesize that thermally modulating the mechanical properties of the outer layer of sliding skin creates friction-induced vibrations without thermal penetration to the thermoreceptor depth, which activate mechanoreceptors and generate haptic perceptions (Fig. 1, A to C). Measurements of friction force between a sliding human finger in contact with a glass film at room and high surface temperature (23° and 42°C, respectively) showed ~50% increase in sliding friction. An analytical mechanical model considers both the temperature dependence of skin viscoelasticity and the moisture level. The decreased viscoelastic modulus at a higher temperature indicates the reduction of skin stiffness. In addition, the moisture level also works as a plasticizer inside the skin, which further reduces the stiffness. It suggests that the increase of finger friction with temperature is due to a reduction in the mechanical stiffness of the finger skin, which causes an increase in the real contact area (Fig. 1E). We further explored the use of localized surface heating to render virtual zones and bumps. Numerical finite element thermal simulations of a sliding finger heated with modulation frequencies up to 250 Hz, combined with known frequency-dependent mechanoreceptor sensitivities, suggest that this technology could be used to render surface textures using miniaturized heater arrays. The proposed method to modulate friction using surface heating is of great interest for a wide variety of human-machine interactions, such as car displays, mobile devices, and touchscreens.

[1]Department of Mechanical Engineering, Texas A&M University, College Station, TX 77843, USA. [2]Department of Mechanical Engineering, The Hong Kong Polytechnic University, Hong Kong, P. R. China. [3]Research Institute for Intelligent Wearable Systems, The Hong Kong Polytechnic University, Hong Kong, P. R. China.
*Corresponding author. Email: y.ma@polyu.edu.hk (Y.M.); cynthia.hipwell@tamu.edu (M.C.H.)
†These authors contributed equally to this work.

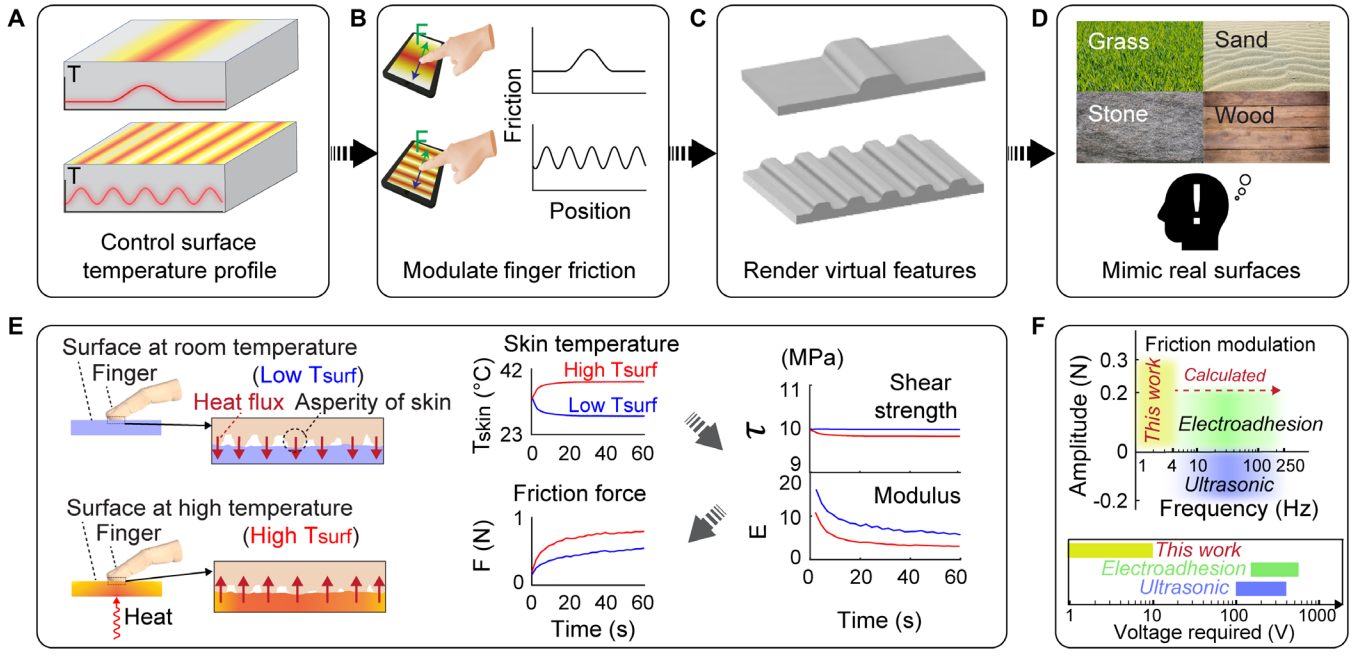

Fig. 1. A schematic of the desired flow map in this work. (**A** to **D**) A schematic of the process to render realistic surfaces. We studied how the different temperature profiles can be used to change the finger friction and thus render the virtual shapes, textures, and potentially realistic surfaces through more psychophysical studies in the future. (**E**) A schematic of the mechanism underlying the temperature effect on the finger friction. The different skin temperatures due to the different surface temperatures induced a change in the interfacial shear strength and viscoelastic modulus of human skin, where the latter was found to be dominant. (**F**) A schematic showing the strength of this work. The method proposed in this work has been demonstrated at low frequency and can generate friction modulation comparable to the existing SHDs but does not require a high voltage.

RESULTS

Effect of surface temperature on friction of fingerpad

To investigate the temperature effect on the friction of a human fingerpad, we used a custom-built experimental setup (*31*) that measures the friction force on a reciprocally moving piece of glass under a controlled normal force and surface temperature as shown in Fig. 2A (see Materials and Methods and fig. S9 for details). Figure 2B shows an example of the variation of the friction force. The friction forces were extracted during stable stage movement (marked by shaded yellow and green areas in Fig. 2C), and the average friction forces at different surface temperatures are shown in Fig. 2D.

The shaded blue and red areas represent ±σ (SD) of the 16 repeated experimental data points of one participant (right index finger of a 32-year-old male) at each surface temperature (23° and 42°C). It can be observed that the friction force was larger at higher surface temperature by ~50% and the rate of increase in the friction force was higher at a higher surface temperature during the early stage of contact (0 to 20 s). Similar behavior was also observed with another participant (fig. S10). The friction force under different surface temperatures, sliding speeds, and normal forces were also measured, and the surface temperature showed the strongest influence over friction force when compared with sliding speed and normal force (fig. S11).

To understand the mechanism underlying the increase in the friction force in response to different surface temperatures, we developed an analytical mechanical model (see text S2 for details). In this analysis, we studied the temperature effect on interfacial shear strength and real contact area, as the friction force is a product of the two variables (eq. S6 in text S2). We first calculated the skin temperature variation with time when the finger makes sliding contact with glass with different surface temperatures (Fig. 1E and fig. S1C) and used the calculated skin temperature to theoretically calculate the interfacial shear strength (text S1). We found that, within the simulated range, the surface temperature affects the shear strength by less than 3%, which cannot explain the 50% change in friction. Therefore, we hypothesized that the main contribution of the temperature effect on friction comes from the change in real contact area in response to surface temperature.

The effect of surface temperature on the real contact area was analyzed using the standard Kelvin-Voigt viscoelastic model, given that the stratum corneum, the outermost layer of human skin, is a viscoelastic material (*32*). In addition, we found that moisture level increases faster when the finger is sliding on a higher temperature surface (fig. S6), which could reduce the modulus of human skin (*33*, *34*). By theoretically deriving a modulus model that incorporates the temperature dependence of skin viscoelasticity and moisture level and fitting it with the modulus calculated using friction data (Fig. 2E), we found lower elasticity and viscosity, and thus shorter time constant, at a higher temperature. This is a general behavior of viscoelastic materials with elevated temperature. In short, our analysis suggests that the physical mechanism behind the change in friction in response to surface temperature has two terms: temperature dependency of both the viscoelastic modulus and moisture level.

Rendering virtual shapes

Minsky *et al.* (*35*) and Robles-De-La-Torre and Hayward (*36*) showed that changes in friction of a two-dimensional (2D) surface can be used to create the haptic illusion of 3D shapes such as bumps and holes. Inspired by this work, we investigated using

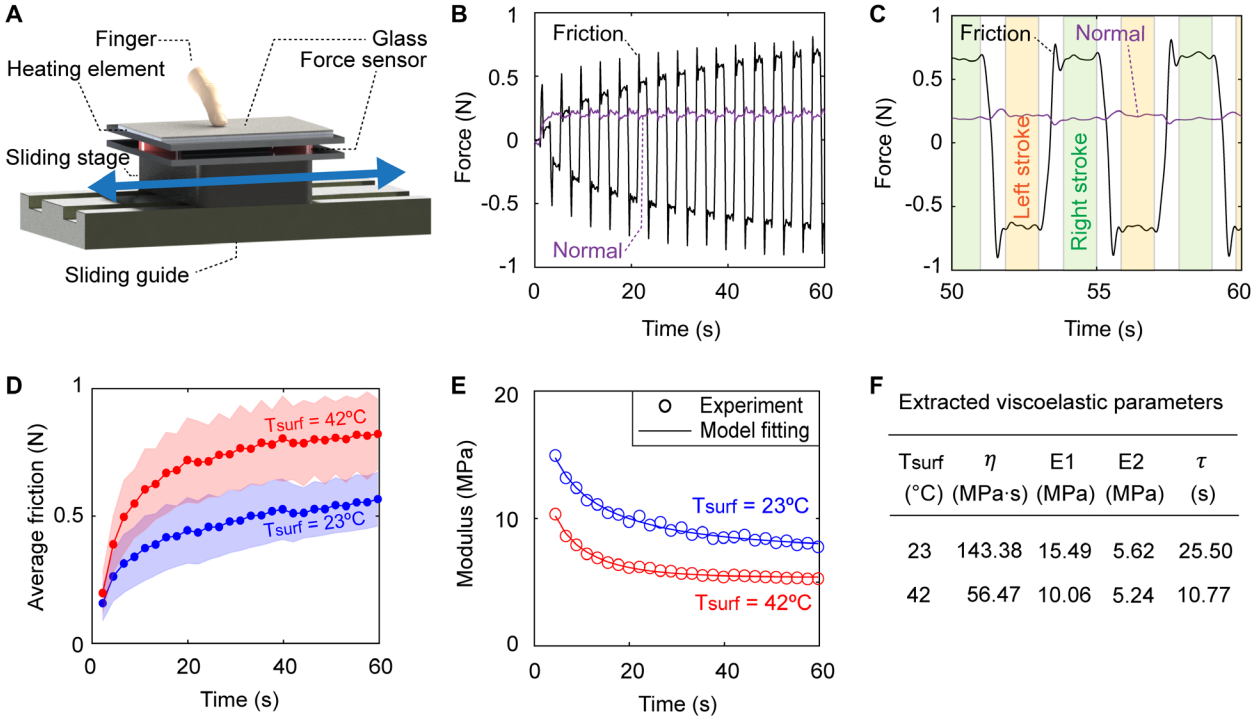

Tsurf (°C)	η (MPa·s)	E1 (MPa)	E2 (MPa)	τ (s)
23	143.38	15.49	5.62	25.50
42	56.47	10.06	5.24	10.77

Fig. 2. Effect of surface temperature on finger friction. (**A**) An illustration of the experimental setup where the stage is reciprocating laterally and the finger is fixed. Force sensors that were sandwiched between two aluminum plates placed on a sliding stage measure the friction and normal forces. (**B**) Friction and normal force with respect to time. The friction force was marked as positive when the stage was moving toward the participant's left-hand side. (**C**) Friction force variation in 10 s, showing the extracted data during stable sliding. (**D**) The averaged friction force at different surface temperatures with respect to time. The shaded area represents twice the SD of 16 repeated data for each surface temperature trial. (**E**) Experimentally estimated and model fits of Moduli of stratum corneum as a function of time. R^2= 0.9789 and 0.9914 for low- and high-temperature cases, respectively. (**F**) Extracted viscoelastic parameters by fitting the model to E_{sc}.

temperature-modulated finger friction to create virtual features such as zones and bumps.

Virtual zoning

A step-like temperature change was generated using two Peltier elements placed beneath a glass sample (Fig. 3, A and B). The numbers ("1" and "2") in Fig. 3B indicate each case of the right or left heater turned on. The left and the right heating elements were turned on separately to heat their surface to 42°C. The time evolutions of the friction force after the onset of touch were averaged every 20 s (Fig. 3, C and D). The friction forces in the different sliding directions were plotted separately to avoid the influence of anisotropy of finger tissue and structure (*37*, *38*). The friction force stepped up during sliding when the finger transitioned from the low- to high-temperature surface and vice versa. The participant reported the feeling of entering or exiting a "sticky" area when the finger was sliding across the borderline of the heating zone.

Virtual bump(s)

Rendering of virtual bump(s) was demonstrated using three polyimide strip heaters spatially separated underneath a glass sample (Fig. 4A). Each heater, when individually turned on, created bump-like temperature profiles (Fig. 4B). The width of the heater used to create a single bump was 25.6 mm, and the width of those used for the three bumps was 12.8 mm. The friction data showed that the friction can be modulated in the same way that the surface temperature varies spatially (Fig. 4C).

For the case of rendering three bumps, the experiment was further performed under different ΔT (Fig. 4D). T_H is the average of the temperature at three upper peaks, and ΔT is the average of the peak-to-peak amplitudes of the temperature profile (Fig. 4B). The normalized change in friction, $\Delta F/F_{off}$, showed a linear relationship with ΔT (Fig. 4D). According to Weber's law (*39*), the ratio of just-noticeable difference, which is represented by the smallest ΔF that a human can perceive, is linearly proportional to the original stimulus F_{off}. In our case, the Weber fraction was found to be approximately 0.2, which was reached at ΔT = 12 to 15°C.

Using our proposed method, the friction force can be modulated up to 0.4 N at a low frequency (1 Hz) and under a large temperature gradient. The maximum friction change of 0.4 N approximately corresponds to the bump height of 6 mm according to the relationship between the lateral force and a Gaussian shaped bump (*36*). In addition, this method can be used to render fine features like textures using a dense array of heaters at a frequency of 250 Hz, corresponding to a wavelength of 400 μm. For magnitude resolution, distinguishable friction force difference can be determined by the Weber fraction (friction difference ΔF/base friction F_{base}) to be ~0.1 N, which was 20% in our study (Fig. 4D) and 10 to 27% in another work (*40*).

To investigate whether different users can perceive the proposed thermo-driven friction modulation, we performed psychophysical experiments. These experiments used the same glass sample as the one that was used in the friction measurement. Three 25.6-mm-wide resistive heaters were mounted underneath the glass sample that was overlaid with a 21-point scale with 5-mm spacing for region identification (see fig. S14A for setup details). This chosen scale

resolution was smaller than the heater width to determine whether the participants were sensitive to the entire heated width or only the edge where the temperature gradient is high.

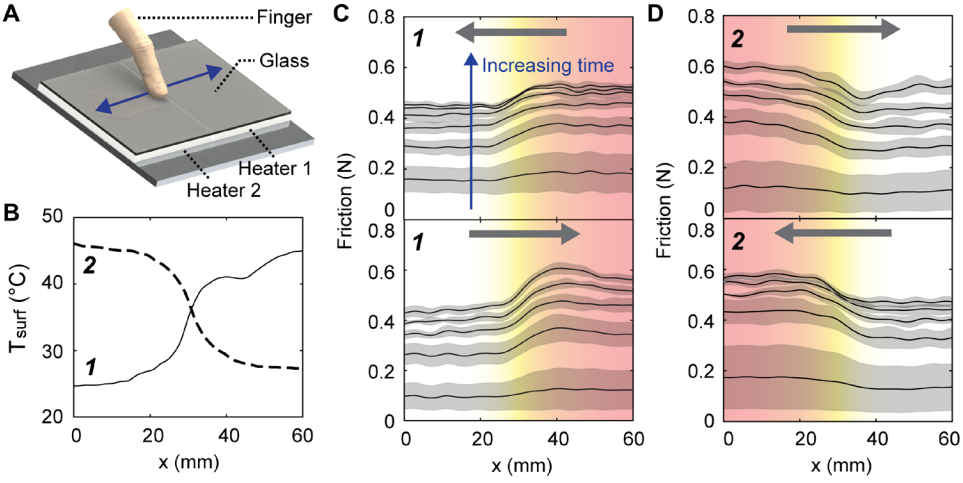

Fig. 3. A demonstration of rendering virtual zones. (**A**) A schematic of virtual zoning experiment. Either heater 1 or 2 was heated to make a "step-like" temperature profile. (**B**) The temperature profiles of two virtual zone scenarios where each heater was turned on individually. (**C** and **D**) Friction force variations of the right and left strokes under different virtual zone definitions. Friction forces for every five strokes in each sliding direction were averaged and plotted together along with a shaded error bar (SD). The five different curves in each subplot are friction forces averaged over different time periods (from bottom to top are 0 to 20, 20 to 40, 40 to 60, 60 to 80, and 80 to 100 s, respectively) increasing with time.

Each experiment consisted of 10 randomly ordered trials: two trials for each heater where it alone was heated to 42 ° C and four control trials where no heater was activated. Before the trials, the participants were asked to slide their index finger on the glass sample with no heater turned on so that they can feel the intrinsic friction of the glass sample. Before the onset of the experiment series, the participants were asked to sit and wait for 5 min to acclimatize themselves in the preset environmental condition to reduce their physiological variation over time (temperature and relative humidity were 23 ± 1°C and 50 ± 2%, respectively). We measured the skin moisture level before each trial. In each trial, the participants were instructed to slide their dominant index finger along the full stroke of the glass sample (100 mm, from #1 to #21 in fig. S14A) until they determine the location of the region that feels differently, if present. Their answer times and skin moisture levels are shown in fig. S14B. The sliding speed was recorded with videos. In each trial, they were asked the following:

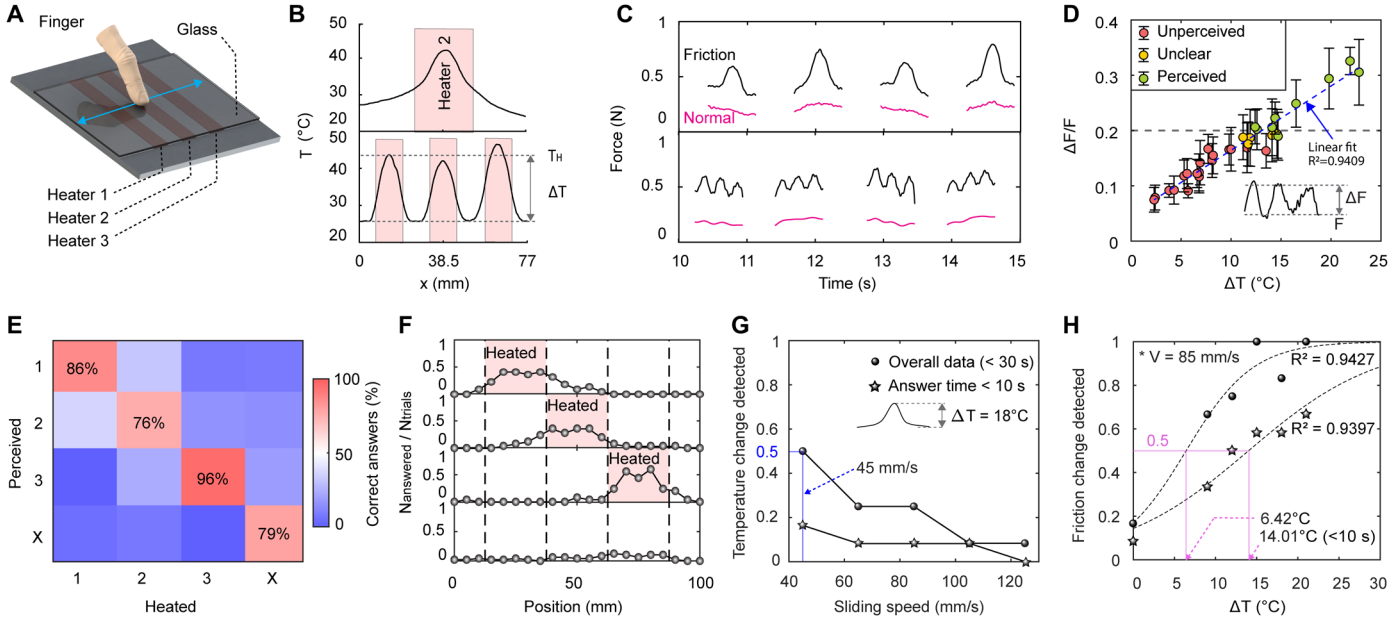

Fig. 4. A demonstration of rendering virtual bumps. (**A**) Schematic of the experiment for rendering virtual bumps. Each heater corresponds to a virtual bump. (**B**) Temperature profiles when a single heater or the three heaters are turned on. (**C**) Friction and normal forces measured with the tribometer for rendering virtual bump(s). (**D**) The ratio of the peak-to-peak amplitude of friction modulation to the average friction versus the peak-to-peak amplitude of the temperature profile. Different marker colors represent different answers for perceiving the virtual bump(s). (**E**) The ratio of the answered numbers to the number of total trials at each location. It represents the relative distribution of the perceived region. (**F**) A confusion matrix at each region that represents whether the participant can identify the heated region with the high friction. (**G**) The proportion of temperature change detected under different sliding speeds. The data were classified into overall data (black circles; answer time was limited to 30 s) and the data that have an answer time of less than 10 s (black stars). The legends presented are also applied to (H). (**H**) The proportion of friction change detected under different Δ*T*. The experimental data were fitted with a sigmoid function to determine the absolute threshold. The data were classified into overall data and the data that have an answer time of less than 10 s.

Before the trial:

1) Are there region(s) in the 21-point scale that feel differently than the rest of the screen?

After the trial:

2) If so, verbally describe the sensation.
3) Did you detect a change in friction?
4) Did you detect a change in temperature?

The participants used the words "high friction," "sticky," "like a bump," etc. to describe the high friction sensation on the heated region (see table S5 for details). The participants were quite adept at perceiving the friction change and identifying the location when one of the regions was heated. The participant answer time was 28 ± 7 s. We plotted the results in the confusion matrix [a matrix that contains information about predicted and actual answers in classification problems (*41*)] shown in Fig. 4E. This matrix shows a high success rate, 76 to 96% for each stimulus, for participants to correctly identify and locate friction modulation within the active heater region. In addition, Fig. 4F summarizes the ratio of the number of positive answers to the total number of trials at each location, highlighting relatively higher proportions on the heated region and lower proportions on the unheated regions. Different participants had different perceived widths and distributions of the heated region (see table S4 for the raw data of answered regions). Hence, it was not clear whether the participants perceived the entire width of the heated region or the edges. Nevertheless, the participants were able to perceive the friction modulation within the correct location.

Note that all 12 participants answered "no" to the question about perceived temperature change after each trial (table S6). We hypothesized that this may be speed dependent, given that the amount of heat transferred between the finger and the heated region is time dependent—the longer the finger stays on the heated region, the larger the total heat transfer. We varied the sliding speed of participants (45 to 125 mm/s) using a metronome and asked before the test to tell whether they could feel any temperature change. The answer time was limited to 30 s, given that the average answer time in the psychophysical experiment for identifying different regions in the previous paragraph was 28 s. In this experiment, the heater at the center was turned on to achieve ΔT = 18°C—a temperature difference between the heated and unheated regions that corresponded to the heated region temperature of 42°C. Figure 4G shows the proportion of temperature change detected under different sliding speeds and ΔT. The stimulus level with a perceived proportion of 0.5 has been widely used in psychometric tests as an absolute threshold (*42*). Therefore, we determined the threshold of sliding speed under which the surface temperature can be perceived. The threshold of the sliding speed for detecting temperature change at ΔT = 18°C was 45 mm/s, which was lower than the average sliding speed (85 mm/s) in the psychophysical experiment for identifying virtual bumps, indicating that people cannot perceive the temperature change at the average sliding speed. The proportion of temperature change detected within 10 s is shown on the right in Fig. 4G, which shows an even lower proportion, meaning that if the users slide their finger for 10 s, then it is unlikely that they will perceive any heat under the given conditions. These results can explain why users cannot perceive the temperature change under the average sliding speed (85 mm/s) and temperature (ΔT = 18°C or T_{Heated} = 42°C) while perceiving the friction modulation. Note that, in Fig. 4G, the proportion of participants who detected temperature change at 85 mm/s was not zero. This was the identical condition for identifying different regions (Fig. 4, E and F) where the participants did not detect the temperature change. Three participants perceived temperature change by reporting "a little warm" after they were asked to specifically detect whether there was any temperature change. On the contrary, without being specifically asked to look for temperature change, they did not feel the temperature change in the experiment. This was probably due to the difference in the participants' attention: When the attention of the participants is devoted to temperature, they may be more sensitive to the change in temperature.

To investigate physically why the participants were not able to perceive the temperature change, we implemented a computational simulation using ABAQUS (see text S1.3 for details). The thermal perception was analyzed on the basis of the temperature of the warm receptor under different contact conditions. When the finger is sliding on a surface where one 25.6-mm-wide heater is turned on to 42°C, the thermoreceptor temperature overall decreased over time, because the skin was cooled down outside of the heated region after being heated up in the heated region. This condition would not activate the warm receptor, which explains why participants did not perceive temperature changes in the heated region. This analysis indicates that judicious use of the thermal mass of the haptic device, in concert with local heaters, can limit the depth of thermal penetration into the skin to limit thermoreceptor activation.

To determine the threshold temperature needed to generate a perceivable friction modulation, we performed another psychophysical experiment where the participants were asked to answer whether they can feel the friction modulation under different temperatures (ΔT = 0°, 9°, 12°, 15°, 18°, and 21°C) during the surface exploration at a sliding speed of 85 mm/s. The rest of the experimental conditions are identical to the ones used in the first psychophysical experiment mentioned above. Their answer times and skin moisture levels are shown in fig. S15. Figure 4H shows the proportion of participants who were able to detect friction change under different ΔT. The data were first fitted with a sigmoid function (*44*), and a threshold temperature difference ΔT for friction detection was determined with a proportion of 0.5, which was 6.42°C. The threshold temperature difference for detecting friction modulation within 10 s was 14.01°C. The answer time for perceiving the friction change was 11 ± 6 s. Note that the answer time recorded here is only the time needed to perceive friction modulation, which was shorter than the time required to both perceive and spatially locate the friction change (28 s) in the psychophysical experiment in Fig. 4 (E and F).

Although the current experimental setup was successful in inducing perception of a series of bumps, the frequency demonstrated above (4 Hz) is not yet high enough to render virtual texture as in other SHDs (*11*, *21*). To examine the theoretical feasibility of rendering virtual textures that stimulate finger surfaces at 100 to 250 Hz (*45*), we developed a 2D numerical heat transfer model during finger sliding (see text S1.4). The skin temperature variation during sliding contact of the fingerpad with the glass sample under different device configurations was further extracted. The simulated skin temperature variation (peak to peak) on the rendered virtual bump(s) (1 and 4 Hz) were 1.6° and 0.7°C, respectively (see fig. S4D). It has been demonstrated that humans can perceive the vibrations of smaller amplitudes at a higher frequency due to the increased sensitivity of mechanoreceptors (*46*, *47*). At 4 Hz, the threshold amplitude of vibration is around 20 μm, whereas at 100 and 250 Hz, the threshold amplitude drops to ~60 and ~20 nm, respectively. Hence, the required amplitude of the friction modulation at high

frequency can be estimated based on the frequency dependency of the threshold. Because we found a linear relationship between the peak-to-peak amplitudes of the surface temperature ΔT and the friction force ΔF (Fig. 4D), the required skin temperature modulation ($\Delta T_{skin,pp,min}$) can be estimated to be ~2.1×10^{-3}°C at 100 Hz and ~0.7×10^{-3}°C at 250 Hz (see text S3). The numerical results showed that the calculated $\Delta T_{skin,pp}$ for both 100- and 250-Hz cases were larger than the required $\Delta T_{skin,pp,min}$ (see fig. S4, F and G), indicating the theoretical possibility of rendering virtual textures at high frequency.

CONCLUSION

In this study, we investigated the effect of surface temperature on finger friction and the feasibility of rendering virtual features using varied temperature profiles as a type of SHD. We found a large effect of surface temperature on finger friction—enough to generate surface haptic effects comparable to current devices and explained by the temperature dependence of both the viscoelasticity and moisture level of human skin. The potential of rendering virtual features was demonstrated by changing the temperature profiles of a glass sample. The friction force was found to vary accordingly with the temperature profile, and psychophysical studies indicated that the users are able to perceive and localize the virtual bump while they did not detect a surface temperature change. The feasibility of high-frequency friction modulation was investigated through modeling, and it was found that it is theoretically possible to render virtual textures using our proposed method. This work shows that surface heating SHDs have great potential in a wide variety of human-machine interfaces.

In its current form, cooling components, such as a water pump and fan, help to better define the desired temperature profiles. This is a challenge that will need to be addressed to miniaturize the device. Although the prototype size could be used in applications such as car displays, future efforts to optimize the design through proper material selection (anisotropic thermal properties), thermal design, and cooling technique would be important to broaden its application to areas such as VR or gaming.

In this study, we performed all experiments under controlled environmental conditions. For application to tactile displays, the effects of different environmental factors such as ambient temperature and humidity, as well as user differences like skin temperature, gender, and age, will be investigated. Future investigations will also focus on the factors affecting temporal variation and methods to initiate the thermo-driven friction modulation more quickly after the user starts sliding the finger. For example, we could use a short heat pulse that is not thermally detectable but can decrease the modulus of the outer layer of skin faster and thus increase friction in a short amount of time. A deeper understanding of variability and design influences will enable the achievement of the device's full potential.

Last, although the focus of this work was to render virtual shapes and textures through friction modulation without thermal sensation, the situation will be more complex in multimodal haptic rendering. Although the entire frequency spectrum of temperature and friction response cannot be attained and the maximum friction modulation amplitude would be decreased at high simulated surface temperature, the mismatch in response times between mechano- and thermoreceptors could be exploited to mimic the effect of many surfaces. For example, a piece of room temperature fabric could be emulated using high-frequency temperature modulation to recreate texture and lower frequency and/or gentle static heating to simulate the reduced thermal transport between skin and fabric relative to the device material. In addition, the surface temperature–induced stiffness reduction discussed here will affect the threshold and magnitude of friction modulation in any multimodal SHD that uses heating, as shown in (*43*), and should be considered in multimodal SHD design.

MATERIALS AND METHODS

The goal of our study was to investigate the feasibility of thermo-driven friction modulation as a method for surface haptic rendering. To perform this study, we built a custom-built tribometer to measure the friction under controlled normal force. We also made a thermal setup to change the temperature and its profile of a glass sample to be able to induce changes in finger friction. In controlled conditions, we investigated the effect of temperature on the finger friction and how different temperature profiles influence the change in friction. We demonstrated a few examples of rendering virtual features such as zones and bumps.

Tribometer

The custom-built tribometer that was used in this study was built to measure the frictional forces under controlled normal force while the stage is reciprocating laterally. It consists of a horizontal linear motor stage (DDS300-E, Thorlabs), a precision linear vertical stage (VP-5ZA, Newport), two six-axis force transducers (Nano43, ATI), and a 3D printed finger holder that restricts the movement of the finger in three directions. A PID (proportional-integral-derivative) control loop for the vertical stage was integrated into the control algorithm in LabVIEW, allowing the vertical stage to compensate for slight movements of the finger and keep a constant normal load. The environmental chamber is equipped with a relative humidity control module that consists of a temperature/humidity controller with an accuracy of 0.5% and a resolution of 0.1% of digital readout and a temperature/humidity sensor (Model 5200-240-230, Model 554, Electro-Tech Systems Inc.), capable of measuring 0 to 100% relative humidity with an accuracy of 2% relative humidity. The normal force was kept 0.2 ± 0.025 N using PID control in all the experiments in this study. The thickness and roughness of the glass sample were 800 μm and 220 nm, respectively.

Thermal setup

An additional experimental setup used to change the surface temperature was mounted on the aluminum plate of the tribometer (see fig. S1). It comprises two Peltier elements (TEC1-12730, BQLZR) to actively heat and cool the glass surface, a water cooling radiator (8541600677, Clyxgs), a water pump (LYSB018E6ZWIQ-ELECTR, Mavel Star), and a water cooling heat exchanger (B07FZWM4Z7, DIYhz) that transfers the heat from the bottom of the Peltier elements to the environment to maintain a constant temperature while preventing the force sensors from thermal drift. To modify the temperature profile, polyimide heaters for rendering bumps and textures (PFH-05/5-16 and PFH-1/5-42 in Fig. 4A; Omega) were used. Two power supplies (TP-3005D-3, Tekpower) were used to input DC power to each part of the setup. During each experiment, thermal infrared images were taken using an infrared thermal imaging camera (T530, FLIR Systems). The emissivity of the thermal imaging was calibrated by comparing the temperature measured by the thermal camera to that by a K-type thermocouple (GG-K-30-500,

Omega) on the same location of the glass sample. The calibrated emissivity of the glass sample was 0.95. The temperature profiles shown in this study were processed data using the MATLAB Image Processing Toolbox and averaging the row values of grayscale thermal images.

Experimental procedures for friction measurements

All the experiments measuring the friction force, including the effect of temperature on finger friction as well as rendering zones, bumps, and textures, were performed under a controlled condition inside an environmental chamber where the temperature was 23° ± 1°C and the relative humidity was 50 ± 2%. Two healthy (31-year-old male and 25-year-old female) participants participated in these experiments. The sliding velocity of the stage was 100 mm/s. Before each experiment, the finger and the glass sample were cleaned with isopropyl alcohol and acclimatized for 10 min to equilibrate the finger with the environment. Before starting the experiment, the moisture level of the fingerpad was measured by Corneometer (CM-825, CK Electronics), the finger was mounted on the finger holder, and then the friction measurement began. After the measurement, the moisture level was measured again. This study was approved by the Institutional Review Board of Texas A&M University (IRB ID: IRB2019-0230D).

Psychophysical experiment

In the psychophysical experiment for identifying the different regions, 12 healthy 21- to 34-year-old participants took part in this experiment (one left-handed and two females). The glass sample and the finger of each participant were cleaned with isopropyl alcohol and acclimatized for 3 min to equilibrate the finger with the environment. Then, one of the three polyimide heaters (PFH-1/5-42, Omega) was heated for the glass temperature to reach 42° ± 2°C, and the participants were asked to actively slide their finger end to end over the glass sample. They were asked to indicate which region feels differently by number(s).

The psychophysical threshold experiments (Fig. 4, G and H) were performed at a different time with 12 healthy 24- to 33-year-old participants (one left-handed and three females). This study was approved by the Institutional Review Board of Texas A&M University (IRB ID: IRB2019-0230D).

When determining the threshold of the temperature difference between heated and unheated region ΔT, the data were fitted with the sigmoid function (*44*)

$$P = \frac{1}{1 + e^{-k(\Delta T - m)}} \quad (1)$$

P is the proportion of the friction change detected. k and m are the fitting parameters. The absolute threshold was determined by taking ΔT at which the proportion $P = 0.5$.

SUPPLEMENTARY MATERIALS

www.science.org/doi/10.1126/scirobotics.abl4543
Texts S1 to S4
Figs. S1 to S15
Tables S1 to S6
References (*48*–*85*)

REFERENCES AND NOTES

1. M. Zhu, Z. Sun, Z. Zhang, Q. Shi, T. He, H. Liu, T. Chen, C. Lee, Haptic-feedback smart glove as a creative human-machine interface (HMI) for virtual/augmented reality applications. *Sci. Adv.* **6**, eaaz8693 (2020).
2. S. Hirche, M. Buss, Human-oriented control for haptic teleoperation. *Proc. IEEE* **100**, 623–647 (2012).
3. A. Chan, K. MacLean, J. McGrenere, Designing haptic icons to support collaborative turn-taking. *Int. J. Hum. Comput. Stud.* **66**, 333–355 (2008).
4. D. Wang, Y. Guo, S. Liu, Y. Zhang, W. Xu, J. Xiao, Haptic display for virtual reality: Progress and challenges. *Virtual Real. Intell. Hardware* **1**, 136–162 (2019).
5. J. Zhong, Y. Ma, Y. Song, Q. Zhong, Y. Chu, I. Karakurt, D. B. Bogy, L. Lin, A flexible piezoelectret actuator/sensor patch for mechanical human–machine interfaces. *ACS Nano* **13**, 7107–7116 (2019).
6. C. Choi, Y. Ma, X. Li, X. Ma, M. C. Hipwell, Finger pad topography beyond fingerprints: Understanding the heterogeneity effect of finger topography for human–machine interface modeling. *ACS Appl. Mater. Interfaces* **13**, 3303–3310 (2021).
7. X. Li, Y. Ma, C. Choi, X. Ma, S. Chatterjee, S. Lan, M. C. Hipwell, Nanotexture shape and surface energy impact on electroadhesive human–machine interface performance. *Adv. Mater.* **33**, 2008337 (2021).
8. X. Yu, Z. Xie, Y. Yu, J. Lee, A. Vazquez-Guardado, H. Luan, J. Ruban, X. Ning, A. Akhtar, D. Li, B. Ji, Y. Liu, R. Sun, J. Cao, Q. Huo, Y. Zhong, C. M. Lee, S. Y. Kim, P. Gutruf, C. Zhang, Y. Xue, Q. Guo, A. Chempakasseril, P. Tian, W. Lu, J. Y. Jeong, Y. J. Yu, J. Cornman, C. S. Tan, B. H. Kim, K. H. Lee, X. Feng, Y. Huang, J. A. Rogers, Skin-integrated wireless haptic interfaces for virtual and augmented reality. *Nature* **575**, 473–479 (2019).
9. C. Basdogan, F. Giraud, V. Levesque, S. Choi, A review of surface haptics: Enabling tactile effects on touch surfaces. *IEEE Trans. Haptics* **13**, 450–470 (2020).
10. A. Akhtar, J. Sombeck, B. Boyce, T. Bretl, Controlling sensation intensity for electrotactile stimulation in human-machine interfaces. *Sci. Robot.* **3**, (2018).
11. R. H. Osgouei, J. R. Kim, S. Choi, Data-driven texture modeling and rendering on electrovibration display. *IEEE Trans. Haptics* **13**, 298–311 (2020).
12. F. Giraud, M. Amberg, B. Lemaire-Semail, Design and control of a haptic knob. *Sens. Actuators A Phys.* **196**, 78–85 (2013).
13. S. Kim, G. Lee, Haptic feedback design for a virtual button along force-displacement curves, in *Proceedings of the 26th Annual ACM Symposium on User Interface Software and Technology* (Association for Computing Machinery, 2013), pp. 91–96.
14. M. Wiertlewski, R. F. Friesen, J. E. Colgate, Partial squeeze film levitation modulates fingertip friction. *Proc. Natl. Acad. Sci. U.S.A.* **113**, 9210–9215 (2016).
15. E. Vezzoli, Z. Vidrih, V. Giamundo, B. Lemaire-Semail, F. Giraud, T. Rodic, D. Peric, M. Adams, Friction reduction through ultrasonic vibration part 1: Modelling intermittent contact. *IEEE Trans. Haptics* **10**, 196–207 (2017).
16. S. Wu, X. Sun, Q. Wang, J. Chen, Tactile modeling and rendering image-textures based on electrovibration. *Vis. Comput.* **33**, 637–646 (2017).
17. Y. Vardar, B. Güçlü, C. Basdogan, Effect of waveform on tactile perception by electrovibration displayed on touch screens. *IEEE Trans. Haptics* **10**, 488–499 (2017).
18. M. Heß, V. L. Popov, Voltage-induced friction with application to electrovibration. *Lubricants* **7**, 102 (2019).
19. D. J. Meyer, M. A. Peshkin, J. E. Colgate, Fingertip friction modulation due to electrostatic attraction, in *Proceedings of the 2013 World Haptics Conference (WHC)*, Daejeon, Korea (IEEE, 2013), pp. 43–48.
20. C. Shultz, M. Peshkin, J. E. Colgate, The application of tactile, audible, and ultrasonic forces to human fingertips using broadband electroadhesion. *IEEE Trans. Haptics* **11**, 279–290 (2018).
21. D. J. Meyer, M. Wiertlewski, M. A. Peshkin, J. E. Colgate, Dynamics of ultrasonic and electrostatic friction modulation for rendering texture on haptic surfaces, in *Proceedings of the 2014 IEEE Haptics Symposium (HAPTICS)*, Houston, TX, USA (IEEE, 2014), pp. 63–67.
22. F. Giraud, T. Hara, C. Giraud-Audine, M. Amberg, B. Lemaire-Semail, M. Takasaki, Evaluation of a friction reduction based haptic surface at high frequency, in *Proceedings of the 2018 IEEE Haptics Symposium (HAPTICS)*, San Francisco, CA, USA (IEEE, 2018), pp. 210–215.
23. M. K. Saleem, C. Yilmaz, C. Basdogan, Tactile perception of virtual edges and gratings displayed by friction modulation via ultrasonic actuation. *IEEE Trans. Haptics* **13**, 368–379 (2020).
24. X. Dai, J. E. Colgate, M. A. Peshkin, LateralPaD: A surface-haptic device that produces lateral forces on a bare finger, in *Proceedings of the 2012 IEEE Haptics Symposium (HAPTICS)*, Vancouver, BC, Canada (IEEE, 2012), pp. 7–14.
25. W. B. Messaoud, F. Giraud, B. Lemaire-Semail, M. Amberg, M.-A. Bueno, Amplitude control of an ultrasonic vibration for a tactile stimulator. *IEEE ASME Trans. Mechatron.* **21**, 1692–1701 (2016).
26. O. Sirin, M. Ayyildiz, B. Persson, C. Basdogan, Electroadhesion with application to touchscreens. *Soft Matter* **15**, 1758–1775 (2019).
27. J. Mullenbach, M. Peshkin, J. E. Colgate, eShiver: Lateral force feedback on fingertips through oscillatory motion of an electroadhesive surface. *IEEE Trans. Haptics* **10**, 358–370 (2017).
28. R. F. Friesen, M. Wiertlewski, M. A. Peshkin, J. E. Colgate, Bioinspired artificial fingertips that exhibit friction reduction when subjected to transverse ultrasonic vibrations, in *Proceedings of the 2015 IEEE World Haptics Conference (WHC)*, Evanston, IL, USA (IEEE, 2015), pp. 208–213.

29. K. Ludema, D. Tabor, The friction and visco-elastic properties of polymeric solids. *Wear* **9**, 329–348 (1966).
30. A. Tiwari, N. Miyashita, N. Espallargas, B. N. Persson, Rubber friction: The contribution from the area of real contact. *J. Chem. Phys.* **148**, 224701 (2018).
31. X. Li, C. Choi, Y. Ma, P. Boonpuek, J. R. Felts, J. Mullenbach, C. Shultz, J. E. Colgate, M. C. Hipwell, Electrowetting: A consideration in electroadhesion. *IEEE Trans. Haptics* **13**, 522–529 (2020).
32. M. Christensen, C. Hargens III, S. Nacht, E. Gans, Viscoelastic properties of intact human skin: Instrumentation, hydration effects, and the contribution of the stratum corneum. *J. Invest. Dermatol.* **69**, 282–286 (1977).
33. C. Barba, C. Alonso, A. Semenzato, G. Baratto, L. Coderch, In vitro DVS approach to evaluate skin reparation. *Cosmetics* **3**, 15 (2016).
34. J. van Kuilenburg, M. A. Masen, E. van der Heide, Contact modelling of human skin: What value to use for the modulus of elasticity? *Proc. Inst. Mech. Eng. J* **227**, 349–361 (2013).
35. M. Minsky, O.-y. Ming, O. Steele, F. P. Brooks Jr., M. Behensky, Feeling and seeing: Issues in force display, in *Proceedings of the 1990 Symposium on Interactive 3D Graphics* (ACM SIGGRAPH Computer Graphics, 1990), pp. 235–241
36. G. Robles-De-La-Torre, V. Hayward, Force can overcome object geometry in the perception of shape through active touch. *Nature* **412**, 445–448 (2001).
37. A. Abdouni, M. Djaghloul, C. Thieulin, R. Vargiolu, C. Pailler-Mattei, H. Zahouani, Biophysical properties of the human finger for touch comprehension: Influences of ageing and gender. *R. Soc. Open Sci.* **4**, 170321 (2017).
38. X. Zhou, J. L. Mo, Y. Y. Li, Z. Y. Xiang, D. Yang, M. A. Masen, Z. M. Jin, Effect of finger sliding direction on tactile perception, friction and dynamics. *Tribol. Lett.* **68**, 85 (2020).
39. E. R. Kandel, J. D. Koester, S. H. Mack, S. Siegelbaum, *Principles of Neural Science* (McGraw Hill, 2001), vol. 4.
40. L. A. Jones, H. Z. Tan, Application of psychophysical techniques to haptic research. *IEEE Trans. Haptics* **6**, 268–284 (2013).
41. A. Santra, C. J. Christy, Genetic algorithm and confusion matrix for document clustering. *Int. J. Comput. Sci. Issues* **9**, 322–328 (2012).
42. M. S. Osmanski, X. Wang, Measurement of absolute auditory thresholds in the common marmoset (Callithrix jacchus). *Hear. Res.* **277**, 127–133 (2011).
43. C. Choi, Y. Ma, S. Sequeira, S. Chatterjee, X. Li, J. R. Felts, M. C. Hipwell, Effect of surface temperature on finger friction and perception in electroadhesion, in *Proceedings of the IEEE World Haptics Conference WHC*, Montreal, QC, Canada (IEEE, 2021), pp. 680–684.
44. N.-J. He, A. R. Horwitz, J. R. Dubno, J. H. Mills, Psychometric functions for gap detection in noise measured from young and aged subjects. *J. Acoust. Soc. Am.* **106**, 966–978 (1999).
45. A. I. Weber, H. P. Saal, J. D. Lieber, J. W. Cheng, L. R. Manfredi, J. F. Dammann, S. J. Bensmaia, Spatial and temporal codes mediate the tactile perception of natural textures. *Proc. Natl. Acad. Sci. U.S.A.* **110**, 17107–17112 (2013).
46. K. O. Johnson, The roles and functions of cutaneous mechanoreceptors. *Curr. Opin. Neurobiol.* **11**, 455–461 (2001).
47. A. Gescheider, S. J. Bolanowski, K. R. Hardick, The frequency selectivity of information-processing channels in the tactile sensory system. *Somatosens. Mot. Res.* **18**, 191–201 (2001).
48. A. Mishra, M. Loomans, J. L. Hensen, Thermal comfort of heterogeneous and dynamic indoor conditions—An overview. *Build. Environ.* **109**, 82–100 (2016).
49. R. S. Prasher, J. C. Matayabas, Thermal contact resistance of cured gel polymeric thermal interface material. *IEEE Trans. Compon. Packag. Technol.* **27**, 702–709 (2004).
50. K. Rykaczewski, Modeling thermal contact resistance at the finger-object interface. *Temperature* **6**, 85–95 (2019).
51. M. Zhang, R. Li, Y. Wu, L. Wang, G. Song, J. Li, Numerical study of the convective heat transfer coefficient of the hand and the effect of wind. *Build. Environ.* **188**, 107482 (2021).
52. F. Chen, H. Nilsson, I. Holmer, Evaluation of hand and finger heat loss with a heated hand model. *Appl. Human Sci.* **18**, 135–140 (1999).
53. M. Ferreira, J. Yanagihara, A transient three-dimensional heat transfer model of the human body. *Int. Commun. Heat Mass Transf.* **36**, 718–724 (2009).
54. H.-N. Ho, L. A. Jones, Modeling the thermal responses of the skin surface during hand-object interactions. *J. Biomech. Eng.* **130**, 021005 (2008).
55. M. Modest, J. Ready, D. Farson, *Handbook of Laser Materials Processing* (Magnolia Publishing Inc., 2001).
56. B. Persson, B. Lorenz, A. Volokitin, Heat transfer between elastic solids with randomly rough surfaces. *Eur. Phys. J. E Soft Matter* **31**, 3–24 (2010).
57. S.-W. Kim, S. H. Kim, C. S. Kim, K. Yi, J.-S. Kim, B. J. Cho, Y. Cha, Thermal display glove for interacting with virtual reality. *Sci. Rep.* **10**, 11403 (2020).
58. S. J. Lederman, R. L. Klatzky, Relative availability of surface and object properties during early haptic processing. *J. Exp. Psychol. Hum. Percept. Perform.* **23**, 1680–1707 (1997).
59. J. Ring, R. de Dear, Temperature transients: A model for heat diffusion through the skin, thermoreceptor response and thermal sensation. *Indoor Air* **1**, 448–456 (1991).
60. D. Gueorguiev, E. Vezzoli, T. Sednaoui, L. Grisoni, B. Lemaire-Semail, The perception of ultrasonic square reductions of friction with variable sharpness and duration. *IEEE Trans. Haptics* **12**, 179–188 (2019).
61. K. O. Johnson, The roles and functions of cutaneous mechanoreceptors. *Curr. Opin. Neurobiol.* **11**, 455–461 (2001).
62. A. Gescheider, S. J. Bolanowski, K. R. Hardick, The frequency selectivity of information-processing channels in the tactile sensory system. *Somatosens. Mot. Res.* **18**, 191–201 (2001).
63. S. Derler, L.-C. Gerhardt, Tribology of skin: Review and analysis of experimental results for the friction coefficient of human skin. *Tribol. Lett.* **45**, 1–27 (2012).
64. M. J. Adams, B. J. Briscoe, S. A. Johnson, Friction and lubrication of human skin. *Tribol. Lett.* **26**, 239–253 (2007).
65. A. Tiwari, N. Miyashita, N. Espallargas, B. N. Persson, Rubber friction: The contribution from the area of real contact. *J. Chem. Phys.* **148**, 224701 (2018).
66. O. Sirin, M. Ayyildiz, B. Persson, C. Basdogan, Electroadhesion with application to touchscreens. *Soft Matter* **15**, 1758–1775 (2019).
67. B. Persson, A. Kovalev, S. Gorb, Contact mechanics and friction on dry and wet human skin. *Tribol. Lett.* **50**, 17–30 (2013).
68. M. J. Adams, S. A. Johnson, P. Lefèvre, V. Lévesque, V. Hayward, T. André, J. L. Thonnard, Finger pad friction and its role in grip and touch. *J. R. Soc. Interface* **10**, 20120467 (2013).
69. B. Persson, Elastoplastic contact between randomly rough surfaces. *Phys. Rev. Lett.* **87**, 116101 (2001).
70. T. André, P. Lefèvre, J.-L. Thonnard, Fingertip moisture is optimally modulated during object manipulation. *J. Neurophysiol.* **103**, 402–408 (2010).
71. T. André, V. Lévesque, V. Hayward, P. Lefèvre, J.-L. Thonnard, Effect of skin hydration on the dynamics of fingertip gripping contact. *J. R. Soc. Interface* **8**, 1574–1583 (2011).
72. A. E. Kovalev, K. Dening, B. N. Persson, S. N. Gorb, Surface topography and contact mechanics of dry and wet human skin. *Beilstein J. Nanotechnol.* **5**, 1341–1348 (2014).
73. J.-H. Park, J.-W. Lee, Y.-C. Kim, M. R. Prausnitz, The effect of heat on skin permeability. *Int. J. Pharm.* **359**, 94–103 (2008).
74. S.-M. Yum, I. K. Baek, D. Hong, J. Kim, K. Jung, S. Kim, K. Eom, J. Jang, S. Kim, M. Sattorov, M. G. Lee, S. Kim, M. J. Adams, G. S. Park, Fingerprint ridges allow primates to regulate grip. *Proc. Natl. Acad. Sci. U.S.A.* **117**, 31665–31673 (2020).
75. E. Sparr, D. Millecamps, M. Isoir, V. Burnier, Å. Larsson, B. Cabane, Controlling the hydration of the skin though the application of occluding barrier creams. *J. R. Soc. Interface* **10**, 20120788 (2013).
76. M. Christensen, C. Hargens III, S. Nacht, E. Gans, Viscoelastic properties of intact human skin: Instrumentation, hydration effects, and the contribution of the stratum corneum. *J. Invest. Dermatol.* **69**, 282–286 (1977).
77. B. Delhaye, P. Lefevre, J.-L. Thonnard, Dynamics of fingertip contact during the onset of tangential slip. *J. R. Soc. Interface* **11**, 20140698 (2014).
78. H. Jayabal, N. Dingari, B. Rai, A linear viscoelastic model to understand skin mechanical behaviour and for cosmetic formulation design. *Int. J. Cosmet. Sci.* **41**, 292–299 (2019).
79. S. Derler, L.-C. Gerhardt, A. Lenz, E. Bertaux, M. Hadad, Friction of human skin against smooth and rough glass as a function of the contact pressure. *Tribol. Int.* **42**, 1565–1574 (2009).
80. B. Persson, Capillary adhesion between elastic solids with randomly rough surfaces. *J. Phys. Condens. Matter* **20**, 315007 (2008).
81. X. Libouton, O. Barbier, L. Plaghki, J.-L. Thonnard, Tactile roughness discrimination threshold is unrelated to tactile spatial acuity. *Behav. Brain Res.* **208**, 473–478 (2010).
82. S. Guest, S. Guest, A. Mehrabyan, G. Essick, N. Phillips, A. Hopkinson, F. Mcglone, Physics and tactile perception of fluid-covered surfaces. *J. Texture Stud.* **43**, 77–93 (2012).
83. C. Basdogan, M. R. A. Sormoli, O. Sirin, Modeling sliding friction between human finger and touchscreen under electroadhesion. *IEEE Trans. Haptics* **13**, 511–521 (2020).
84. S. Derler, R. Rossi, G.-M. Rotaru, Understanding the variation of friction coefficients of human skin as a function of skin hydration and interfacial water films. *Proc. Ins. Mech. Eng. J* **229**, 285–293 (2015).
85. T. Kamei, T. Tsuda, S. Kitagawa, K. Naitoh, Koji Nakashima, T. Ohhashi, Physical stimuli and emotional stress-induced sweat secretions in the human palm and forehead. *Anal. Chim. Acta* **365**, 319–326 (1998).

Funding: We acknowledge the Texas A&M Office of the President X-Grant Program: Mastering Friction to Reduce Current and Future Energy Demands, Texas A&M University and Texas A&M Engineering Experiment Station startup funds, the Governor's University Research Initiative, the Chancellor's University Research Initiative, H. Frost, and the J. Mike Walker '66 Department of Mechanical Engineering Graduate Student Summer Research Grant Program.
Author contributions: Conceptualization: J.R.F. and M.C.H. Methodology: C.C., Y.M., and R.F.F. Validation: C.C., X.L., S.C., and S.S. Formal analysis: C.C. and Y.M. Investigation: C.C., Y.M., X.L., and S.S. Data curation: C.C. and Y.M. Writing—original draft: C.C. and Y.M. Writing—review

and editing: C.C., Y.M., R.F.F., J.R.F., and M.C.H. Visualization: C.C. and Y.M. Supervision: J.R.F. and M.C.H. Project administration: J.R.F. and M.C.H. Funding acquisition: M.C.H. **Competing interests:** M.C.H. is a member of the Scientific Advisory Board of Tanvas Inc., whose technology is in the general field of surface haptics, but the company is not involved in the development of nor does it have ownership of this technology. C.C., M.C.H., Y.M., and J.R.F. are inventors on a patent application related to this work (provisional application 2238-16900, "Systems and method for providing tactile feedback to a user"). The authors declare that they have no other competing interests. **Data and materials availability:** All data needed to evaluate the conclusions in the paper are present in the paper or the Supplementary Materials.

Submitted 15 July 2021
Accepted 31 January 2022
Published 23 February 2022
10.1126/scirobotics.abl4543

Science Robotics

Surface haptic rendering of virtual shapes through change in surface temperature

Changhyun Choi, Yuan Ma, Xinyi Li, Sitangshu Chatterjee, Sneha Sequeira, Rebecca F. Friesen, Jonathan R. Felts, and M. Cynthia Hipwell

Sci. Robot. **7** (63), eabl4543. DOI: 10.1126/scirobotics.abl4543

Science Robotics (ISSN 2470-9476) is published by the American Association for the Advancement of Science. 1200 New York Avenue NW, Washington, DC 20005. The title *Science Robotics* is a registered trademark of AAAS.